Nanoscale

Accepted Manuscript

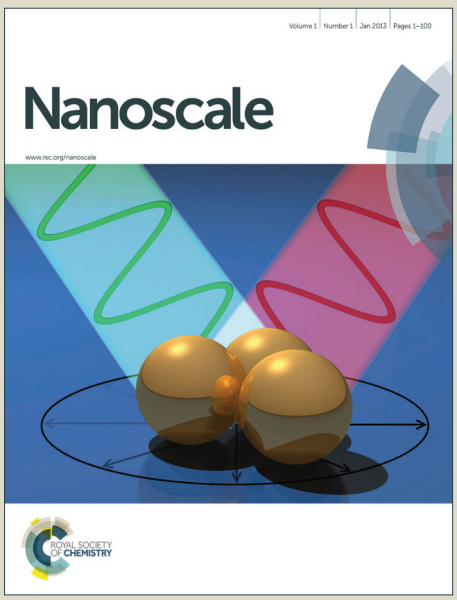

ROYAL SOCIETY OF CHEMISTRY

www.rsc.org/nanoscale

WS_2 nanosheet as a new photosensitizer carrier for combined photodynamic and photothermal therapy of cancer cells

Yuan Yong[a§], Liangjun Zhou[ac§], Zhanjun Gu[a]*, Liang Yan[a], Gan Tian[ad], Xiaopeng Zheng[ac], Xiaodong Liu[e], Xiao Zhang[ab], Junxin Shi[af], Wenshu Cong[a], Wenyan Yin[a]*, Yuliang Zhao[ab]*

[a]Key Laboratory for Biomedical Effects of Nanomaterials and Nanosafety, Institute of High Energy Physics, Chinese Academy of Sciences, Beijing, 100049, P. R.China.

[b]Key Laboratory for Biomedical Effects of Nanomaterials and Nanosafety, National Center for Nanosciences and Technology of China, Beijing, 100190, P. R. China.

[c]College of Materials Science and Opto-Electronic Technology,
University of Chinese Academy of Sciences, Beijing, 100049, P. R. China.

[d] College of Chemistry, Sichuan University, Chengdu, 610064, P. R. China

[e]College of Environmental and Chemical Engineering, Yanshan University, Qinhuangdao, 066004, P. R. China.

[f]Department of Material Physics &. Chemistry，College of Materials Science & Engineering, Huaqiao University, Xiamen 361021, P. R. China.

*Correspondence: zjgu@ihep.ac.cn, zhaoyuliang@ihep.ac.cn, yinwy@ihep.ac.cn

[§] These authors contributed equally.

Abstract

We developed a simple and efficient strategy to fabricate the WS_2 nanosheets with low toxicity and well water solubility via a liquid exfoliation method by using H_2SO_4 intercalation and ultrasonication. The as-prepared WS_2 nanosheets were employed not only as the NIR absorbing agent for photothermal therapy (PTT) but also as the photosensitizers (PSs) carrier for photodynamic therapy (PDT) due to its sheet like structure that enable large surface area to load PSs molecules. Moreover, singlet-oxygen generation of PSs-WS_2 complex could be finely controlled by NIR irradiation that could manipulate the PSs release behavior from WS_2 nanosheets. The synergistic anti-tumor effect of WS_2 nanosheets mediated PDT-PTT were also

evaluated carefully and the results clearly showed that the efficacy of combined PDT-PTT treatment of cancer cells is significantly higher than PDT only and PTT only treatment，indicating the enhanced efficiency of the combined therapeutic system. In addition, the WS_2 could be used as the computed tomography (CT) contrast agent for bio-imaging since W atoms have strong X-ray attenuation ability, making them become a multifunctional theranostic platform for simultaneous imaging-guided diagnosis and therapy.

Key words: nanosheets, nanocarriers, photothermal therapy, photodynamic therapy, synergistic anti-cancer effect

Introduction

Phototherapy including photothermal and photodynamic therapy has increasingly attracted much attention for the treatment of various cancers due to its many advantages such as low cost, highly localized and specific tumor treatment, fewer side effects compared with radiation therapy and chemotherapy, outpatient therapy and minimal trauma to organism tissues. [1] This type therapy used photosensitizers (PSs) and light irradiation to eradicate target tumors. For photothermal therapy (PTT), the photosensitizer is usually a kind of optical absorbing agent with strong near infrared (NIR) absorbance that has the capability to efficiently convert the photo energy into heat to kill cancer cells under NIR irradiation.[2-3] While, in the process of photodynamic therapy (PDT), the photo energy could be transferred from photosensitizers to the surrounding oxygen molecules, resulting in the generation of cytotoxic oxygen-based molecular species such as $^1O_2$ to induce cell death and tissue destruction.[4-5] Recently, the emergence of nanomaterials offers new opportunities to improve the therapeutic efficacy or overcome the limitations in the current PTT and PDT. [6-10] For example, PSs molecules for PDT are usually composed of lipophilic compounds that show poor water solubility, resulting in the aggregation of PSs molecules in blood plasma. Nanoscaled materials could be used as efficient PSs carriers to facilitate the delivery of PSs due to their better hydrophilicity and appropriate size for passive targeting tumor tissues through the enhanced permeability

and retention effects (EPR). [11-17] Some of nanomaterials such as gold nanoparticles, [18-26] carbon nanomaterials [27-30] and copper sulfide [31-36] have been widely employed as PTT agents, which could efficiently convert the light into heat and thus induce hyperthermia to tumor tissues without damaging adjacent healthy tissues showing reduced side effects and improved selectivity. Although impressive advances have made in nanoscale PSs agents for PTT and PDT, the types of nanomaterials combing both PDT and PTT capabilities simultaneously are limited. Combined phototherapies (PDT and PTT) based on one nanoplatform may exceed the individual therapeutic efficacy of each system and lead to enhanced therapeutic outcome. [37-42] Therefore, there is still a great demand for developing new nanomaterials for combining the photodynamic and photothermal therapy to realize synergistic anti-cancer effects.

Very recently, two-dimensional (2D) nanoscaled transition-metal dichalcogenides, such as MoS_2 and WS_2, have been used as a new NIR absorbing agent for PTT ablation of cancer in vitro and in vivo. [43-45] For example, in the latest report, Liu et al for the first time demonstrated the potential of WS_2 for highly effective in vivo photothermal ablation of tumors in a mouse model. [43] Moreover, since tungsten has the strong X-ray attenuation ability, the application of WS_2 nanosheets could also extend to be used as an X-ray computed tomography (CT) contrast agent for bio-imaging of tumor. [43] Apart from its potentials for PTT and bio-imaging, WS_2 nanosheet may also act as a drug delivery carrier, which is ideal for drug loading through physical interaction or chemical conjugation due to its sheet like structure that enable it has high surface area. Therefore, the WS_2 nanosheet could be an ideal multifunctional platform for simultaneous bio-imaging and combined PDT-PTT therapy of cancer. However, no studies have been reported for WS_2 nanosheets mediated delivery of photosensitizers and also no research have been done to evaluated the synergistic anti-tumor effect of WS_2 nanosheets mediated PDT-PTT.

In this work, we for the first time use BSA coated WS_2 nanosheets as photosensitizers carriers for combined PDT and PTT. The as-obtained WS_2-PS complex showed enhanced anticancer effects in vitro by the combination of photothermal and photodynamic therapy. Interestingly, we also found that the singlet-oxygen generation

(SOG) by PSs could be effectively controlled by NIR irradiation that could manipulate the PSs release behavior from WS_2 nanosheets. When PSs (MB) are absorbed on the surface of WS_2 nanosheets, the energy transfer from PSs to WS_2 is effective, and the SOG could be efficiently inhibited by WS_2 due to its high optical absorption. Upon NIR irradiation, WS_2 converts the optical energy to heat, which results in the efficient release of PSs from WS_2 nanosheets. Thus, the efficiency of $^1O_2$ production is remarkable recovered. (Scheme 1) This feature makes WS_2 nanosheets become a smart platform for the controllable regulation of photo activity of PSs, which may improve the efficacy and selectivity of phototherapy and reduced the unwanted collateral damage to surrounding normal tissues. Moreover, WS_2 nanosheets also showed strong X-ray attenuation, which provided the potential for CT bio-imaging. Therefore, the as-prepared WS_2 nanosheets offer a new possibility in exploring the multifunctional nano-platform for simultaneous biomedical imaging and combined PDT and PTT.

MATERIALS & METHODS

Materials

Commercial tungsten disulfide (WS_2, 99.8 %), and Methylene blue (MB, biological stain) were all obtained from Alfa Aesar and used without further purification. Sulfuric acid (H_2SO_4, 95.0 %~98.0 %, analytical reagent) was adopted from Beijing Chemical Corporation. Bovine serum albumin (BSA) was obtained from Amerso Company. Singlet Oxygen Sensor Green reagent (SOSG, molecular probe) was supplied by Life Technology Company. Dulbecco's Modified Eagle Medium (DMEM) and fetal bovine serum (FBS) were obtained from Gibco Company. Calcein-AM (CA)-Propidium Iodide (PI) stain and Cell Counting Kit-8 (CCK-8) were all provided from Dojindo Laboratories. Deionized (DI) water was used in the whole process.

Preparation of mono/few layer of WS_2 Nanosheets:

Commercial WS_2 powder was first ground by grinding miller for 2 h. Subsequently, the WS_2 (40 mg) powder was dispersed in 40 mL of sulfuric acid (H_2SO_4, 95.0%~98.0%) for intercalation 24 h at the temperature of 90 □. The as-prepared

products were collected by centrifugation and washed with DI water for several times to remove the residual H_2SO_4. Then, the H_2SO_4-intercalated WS_2 were dispersed into 40 mL of DI water under bath-sonication for 20 min. Finally, the solutions were probe-sonicated at a power of 325 W for 2 h. The mono/few layer WS_2 nanosheets were obtained by centrifugation and washed with DI water. The yield of the as-prepared WS_2 nanosheets is calculate to be 90%.

Surface modification of WS_2 nanosheets with BSA

To make the synthesized WS_2 nanosheets applied in the biological system, BSA was modified on the surface of WS_2 nanosheets. In a typical synthesis, 60 mg of BSA was mixed with 3 mL of WS_2 (2 mg/ mL) aqueous solution and then stirred for 3 h at room temperature. The as-synthesized BSA-WS_2 nanosheets were collected by centrifugation at 12,000 rpm for 5 min. Finally, the precipitation was re-dispersed in DI water and stored at 4 ℃ for further experiments.

Loading and release behaviors of Photosensitizer Methylene Blue：

To investigate MB loading capacity, MB solution with different concentrations (250, 200, 150, 100, 50 and 25 μM) was slowly added into BSA-WS_2 dispersion and then the mixture was magnetically stirred overnight at room temperature without light irradiation. After that, unloaded MB was removed by centrifugation and washed with DI water. The amounts of MB loaded on the BSA-WS_2 nanosheets surface was determined by the change at its characteristic peak absorption of 665 nm using UV-Vis spectroscopy.

Singlet oxygen measurement

In a typical experiment, singlet oxygen sensor green (SOSG), which was highly sensitive to singlet oxygen ($^1O_2$), was employed as molecular probe to detect the singlet oxygen through fluorescence detection. 2.5 μM of SOSG were mixed with different samples, and then irradiated by 808-nm laser (1 W/cm^2), 665-nm LED lamp (0.05 W/cm^2) or the both of them used at the same time for different time. The generation of $^1O_2$ was measured via detecting the increasing intensity of SOSG photoluminescence (PL) emission band at 530 nm, when using the characteristic peak absorption of SOSG at the excitation of 494 nm.

NIR Laser Photothermal Effect of WS_2 nanosheets

To investigate the photothermal effect of as-prepared WS_2 nanosheets, different concentrations of WS_2 nanosheets were irradiated by 808-nm NIR laser at a power density of 1 W/cm^2 for 10 min. The temperature of the solution was detected by using an IR thermal camera at each time point. Meanwhile, to evaluate the impact of NIR laser power density, the concentration of WS_2 was kept at 50 μg/ mL while different power density (1.0, 0.8, 0.5, 0.3 W/cm^2) was used to irradiate for 10 min, with no change of other experimental conditions. DI water was applied as a negative control.

Cytotoxicity Evaluation and Luminescence Microscopy Imaging *In Vitro*

HeLa cells (Human cervical cancer cells) were chosen and cultured in a 96-well culture plate at a density of 2×10^4 per well. The cells were seeded in DMEM (High Glucose) culture medium containing 10% fetal bovine serum (FBS, GIBCO) at 37 ℃ under a humidified atmosphere with 5% CO_2. After 24 h incubation, the cells were treated with different concentrations of WS_2 or BSA-WS_2 and co-incubated for another 24 h without light interference. Then the culture medium was removed and washed twice with PBS. Subsequently, 100 μL of fresh DMEM medium containing CCK-8 (10 %) was added and further incubated for 1 h at 37 ℃ and finally the absorbance of the samples with fresh DMEM was measured at the characteristic peak of 450 nm using the microplate reader (Thermo scientific, MULTISCAN MNK3).

For combining PTT and PDT effects *in vitro*, HeLa cells were incubated in a 6-well culture plate at a density of 2×10^4 per well. After that, HeLa cells were treated with BSA-WS_2, MB or BSA-WS_2@MB complex for 24 h. The concentration of BSA-WS_2 and MB was fixed at 100 μg/ mL and 3.5 μg/ mL, respectively. Subsequently the culture medium was removed and washed twice with PBS and replaced by fresh DMEM medium. Then the cells treated with BSA-WS_2, MB or BSA-WS_2@MB complex were irradiated by an 808-nm laser (15 min), 665-nm LED lamp (5 min) or both of them used at the same time. After incubating for 12 h, the culture medium was washed twice with PBS and stained with CA-PI for 15 min, then washed twice with PBS again and then the luminescence images were acquired using an inverted

luminescence microscopy (OLYMPUS X73, JAPAN).

CT imaging *in vitro and in vivo*

Different concentrations of BSA-WS_2 were dissolved in 0.5% agarose gel solution which were set in the 1.5 mL centrifuge tubes for further phantom tests . And the Iopromide with the same concentrations were used as the control experiments for comparison. The CT imaging *in vitro* was accomplished on the Gamma Medica-Ideas. Imaging parameters were as follows: field of view, 1024 pixels × 1024 pixels; effective pixel size, 50 μm; 80 KV, 270 μA. The Hounsfield unit values and CT images *in vitro* were analyzed by Triumph ™ X-O ™ CT system. And the CT imaging *in vivo* was performed by SIEMENS CT imaging system (Inveon Gantry LG CT).

Characterization

Transmission electron microscopy (TEM, Tecnai G^2 20 S-TWIN) was employed to obtain the morphologies and size of the samples. The height of the samples was measured using atomic force microscopy (AFM, Agilent 5500, Agilent, USA). The crystal phase was obtained from X-ray powder diffractometer (XRD, Japan Rigaku D/max-2500 diffractometer) with CuK_α radiation (λ = 1.54056 Å). Stability photographs were taken with a Nikon D3100 digital camera. The UV-Vis absorption spectra were recorded on a UV-Vis spectrophotometer (U3900, Hitachi). The temperature curve was recorded and Infrared thermal images were taken by using a thermal imaging camera (E40, FLIR). Photoluminescence of SOSG was obtained by a fluorescence spectrophotometer (Horiba Jobin Yvon FluoroLog3). The luminescence microscopy images were taken by an inverted luminescence microscopy (OLYMPUS X-73, JAPAN).

Results and discussion

The WS_2 nanosheets were synthesized via a liquid exfoliation method by using H_2SO_4 intercalation and ultrasonication, which broke the van der walls interaction forces in bulk WS_2 to give mono and few layer nanosheets (scheme 1). Compared to previous reported Li ions insertion method for preparing WS_2 nanosheets, [43] the method

presented here is insensitive to air and water and thus can potentially be scaled up to produce large quantities of exfoliated WS_2 nanosheets. AFM analysis (Fig. 1a) showed that the average thickness of as-obtained WS_2 nanosheets was about 1.6 nm, indicating the formation of mono and few layer nanosheets from WS_2 bulk. The crystal structure and purity of the fabricated WS_2 were measured by XRD. As shown in Fig 1d, all peaks exhibit the characteristics of the hexagonal WS_2 (JCPDS card No. 08-0237). No other impurities were found, revealing the high purity of the as-obtained product. TEM images (Fig. 1c) confirmed its sheet like structure with diameters of 20-100 nm. In order to improve its bio-compatibility and dispersibility in physiological solution, the as-prepared WS_2 was further functionalized with BSA through physical absorption. After the surface coating with BSA, the thickness of WS_2 nanosheets increased to 4-5 nm (Fig. 1b), mainly due to the attachment of BSA on both planes of WS_2 nanosheets. The FT-IR further confirmed the existence of BSA on the WS_2 nanosheets (Fig. 1e). The as-prepared BSA-WS_2 exhibited well dispersibility in PBS. (Fig. S2)

The aqueous solution of BSA-WS_2 showed a brown color with a strong absorption in the UV to NIR region. (Fig. 1f) The extinction coefficient of BAS-WS2 nanosheets at 808 nm was determined to be 21.8$Lg^{-1}cm^{-1}$, which was higher than that of Au nanorod (a commonly used PTT agent). [18, 21, 26, 46] Thus, this kind of nanoparticles has the potential as photothermal agents. Next, we evaluated the photothermal effect of WS_2 nanosheets with different concentrations upon the irradiation of 1 W/ cm^2 808 nm laser for 10 min (Fig. 2a)**.** Pure water was used as a negative control. With the addition of WS_2 nanosheets, the temperature of WS_2 contained solution increased with the irradiation time, and the temperature increased more rapidly with increasing the concentration of WS_2 nanosheets. For example, the temperature of the solution containing 450 μg/ mL WS_2 rose from 25 °C to 55 °C after NIR irradiation for 10 min. In contrast, the pure water only increased 2 °C under the similar experimental condition. Furthermore, we found that the photothermal heating effect of WS_2 nanosheets was laser power intensity-dependent (from 0.3 to 1.0 W/cm^2) (Fig. 2b). With the increase of the NIR laser power density, the temperature of the photothermal

material became higher. The photothermal conversion efficiency (η value) was calculated to be 32.83 % based on Eq. 1 [47] (see the supporting information for details).

$$\eta = \frac{hs(T - Tsurr) - Q_{Dis}}{I\left(1 - 10^{-A808}\right)} \quad (1)$$

The η value of WS_2 is comparable with that of Au nanorod, [22-25] indicating the as-prepared BAS-WS_2 was suitable for using as PTT agent (Fig. 2c&d).

As considering its sheet like structure and relevant high surface area, the WS_2 nanosheets are also expected to be drug carriers for drug delivery. In this work, we at first time use WS_2 nanosheets for loading and delivery of PSs for combined PDT and PTT. MB was chosen as the model PS because of its high photosensitizing efficacy and low dark toxicity. [48] The surface functionalization of BSA not only improves their dispersibility but also offers the capability to load MB on the surface of WS_2. Due to BSA's amphilic molecule structure, it allowed the tight absorption of lipophilic PS molecules. [49] Thus, MB could be easily loaded on the surface of WS_2 by simply physical mixing. The saturated loading capacity for MB in PBS was determined to be 0.1mmol/g by measuring the characteristic absorption peak of MB at 665 nm (Fig. 3a). Therefore, it could be concluded that BSA-WS_2 has promising potential for PS delivery.

The release behavior of MB from WS_2 in PBS was also investigated and a low leakage within 10 % of MB escaped from WS_2 after 24 h incubation was observed, revealing the good stability of these BSA-WS_2@MB complexes for further biological application. Interestingly, the release of MB could be greatly accelerated by NIR irradiation. As shown in Fig. 3b, the NIR irradiation (808nm, 1W/cm^2) apparently enhanced the cumulative release of MB at different time, which ascribes to photothermal effect of WS_2 nanosheest since increasing local temperature would dissociate the interactions between MB and WS_2 nanosheets and thus more MB molecules are detached from the nanocarriers. For example, the cumulative release of MB with NIR irradiation was about 8 fold higher than that without NIR irradiation. That means the photothermal effects of WS_2 could finely controlled the release behavior of MB from WS_2 nanosheets.

The efficient generation of cytotoxic singlet oxygen plays a key role in photodynamic therapy. We thus investigate the singlet oxygen generation of BSA-WS_2@MB complex upon the irradiation of a 665 nm LED lamp. The singlet oxygen sensor green (SOSG) was employed as a detector to measure the generation of singlet oxygen，which reacted irreversibly with singlet oxygen and cause an enhancement of SOSG fluorescence at 530 nm. [2] BSA-WS_2 only, free MB and BSA-WS_2@MB complex were mixed with SOSG, respectively and then illuminated under a 665 nm LED lamp excitation at different intervals. As shown in Fig. 3c, BSA-WS_2 only has no obvious ability to produce singlet oxygen since the fluorescence intensity of SOSG remained unchanged. In the contrast, when free MB was exposed to the 665 nm LED lamp, a significant increase of emission intensity of SOSG was observed. BSA-WS_2@MB also produced singlet oxygen but the amount was much lower than the free MB under similar condition. The reason for this phenomenon may be that WS_2 could efficient quench the singlet oxygen generation (SOG) of MB due to its high optical absorption and efficient energy transfer from MB to WS_2 nanosheets. Fortunately, the photoactivity of PSs could be restored by introducing the NIR irradiation. As shown in Fig. 3c, after the irradiation of 808 nm laser for 10 min, the SOG greatly enhanced since the intensity of SOSG increased 5 fold than that without NIR irradiation. These results inspired us that the as-obtained BSA-WS_2@MB complex could be employed as a smart platform for controllable singlet oxygen generation. During the delivery process, the singlet oxygen generation of MB absorbed on WS_2 surface was greatly inhibited. When these nanoparticles arrived at the target tissues, the photoactivity of PSs was quickly recovered after introducing the NIR irradiation, which disturbed the interaction between MB and WS_2 nanosheets eventually resulting in the release of MB form WS_2. This may improve the PDT selectivity to tumor while leaving healthy tissues unharmed. Moreover, therapeutic efficacy of BSA-WS_2@MB complex could be further enhanced by addition NIR induced PTT.

Before we move on to demonstrate the phototherapy effect of BSA-WS_2@MB complex, we evaluated the cytotoxicity characteristics of WS_2 before and after BSA coating, which is a very important issue towards the medical applications of such

materials. The standard Cell Counting Kit-8(CCK-8) assay was used to determine the relative cell viability of HeLa cells after they were incubated with WS_2 and BSA-WS_2 at various concentrations for 24 h (Fig. 4a). No significant cytotoxicity of WS_2 nanosheets was observed even at high concentrations up to 0.2 mg/ mL, where the cell viability of HeLa cells is still higher than 85%. In contrast, the WS_2 nanosheets prepared by Li ions insertion method have been reported to have obvious toxic at the similar condition. [43] The reason for the lower toxicity of our obtained WS_2 nanosheets may be that we prepared these WS_2 nanosheets in a mild aqueous solution without using any toxic organic solvents and chemicals. So the strategy presented in this work is much 'green' for the fabrication of WS_2 nanosheets with low toxicity, benefiting their further bio-applications. BAS coated WS_2 nanosheets also show very lower toxicity since BSA molecules are well known biocompatible.

Next, in vitro phototherapy effects of the PTT, PDT and combined PDT-PTT were evaluated by incubating HeLa cells. For PTT test, the cells were incubated with BSA-WS_2 for 2 h and then exposed to an 808 nm laser at 1 W/cm^2 for 10 min. After the treatment, the cell viability was determined by CCK-8. As presented in Fig. 4b, the cell viability gradually decreased with an increase of laser power output, indicating the NIR induced photothermal killing of cancer cells. For PDT effect evaluation, BSA-WS_2@MB and free MB were incubated with HeLa cells for 2 h and then irradiated by a 665 nm LED lamp at 50mW/ cm^2 for 3 min, respectively. The power and dose of the 665 nm light were very low and thus could not cause any obvious heating effect of WS_2. So the cell destruction is contributed to the PDT effect of BSA-WS_2@MB complex. As shown in Fig. 4c, upon 665 nm light excitation, the BSA-WS_2@MB complex could kill the cancer cells but its efficacy is lower than that of free MB at same condition since the WS_2 inhibit the singlet oxygen generation by their quenching effects as mentioned above. However, by introduction of the 808 nm irradiation, the cancer cells killing ability of BSA-WS_2@MB complex was greatly enhanced, resulting in much lower remaining cell viability compared to those after mono-therapy with 665 nm LED only treatment or with 808 nm laser only treatment. These results clearly confirm the enhanced therapeutic performance of

BSA-WS_2@MB complex by combining both PTT and PDT. The reason for the enhancement of therapeutic efficacy may be that under NIR irradiation, the photothermal effects of WS_2 accelerated the release of PS from carriers and then recovered the singlet oxygen generation of PSs, resulting in improved PDT effects for killing cancer cells. Moreover, the phothothermal effect caused by WS_2 nanosheets also enhanced the anticancer efficacy.

To further demonstrate the phototherapy effects of PTT-PDT combined treatment on cancer cells, intuitive visual results are observed by the experiment of live-dead cell staining. As shown in Fig. 5, survival situations of the HeLa cells are illustrated by staining them with fluorescence dyes-green indicating live cells and red representing the dead ones. In the absence of WS_2 or MB, the 808 nm NIR laser and 665 nm LED light did not caused obvious damage to cells. As shown in Fig. 5d, the PTT only treatment could kill the cancer cells and its efficacy is a little higher than that of PDT only effect (Fig. 5e). The combined effects of PDT followed by PTT treatment as illustrated in Fig. 5f induced significant higher cell death than PDT only or PTT only treatment, indicating the enhanced efficiency of the combined therapeutic system. These results are well in agreement with the cell viability assay as mentioned above.

Because WS_2 nanosheets contained high atomic number element (W ions) that has strong X-ray attenuation ability, they could be used as X-ray computed tomography (CT) imaging contrast agent. A series of the CT images obtained with 6 gradient concentrations of BSA-WS_2 dispersed in 0.5 % agarose gel solution in the range of 0-10 mg/ mL. The same series of concentration of Iopromide (a commercial used CT contrasts agents) were also used for comparation with the WS_2 nanosheets. As shown in Fig.6a & b, with the increase of BSA-WS_2 concentrations, a sharp signal enhancement and continuous increase of the CT numbers called Hounsfield units were clearly observed. We also founded that the slope of Hounsfield units of BSA-WS_2 was about 36.19 HU L/g, which was much higher than that of Iopromide (20.10 HU L/g) at the same concentration. Then, the CT imaging *in vivo* was also carried out by using BSA-WS_2 nanosheets to further evaluate its potential for using as a CT imaging agent. A Balb/c nude mice bearing HeLa tumors was intratumorally

injected with BSA-WS_2 nanosheets (3 mg/ mL, 50 μL) and then imaged under a CT imaging (SIEMENS, Inveon Gantry LG CT) (Fig. 6c). Strong signals from WS_2 at tumor site in the CT image were clearly observed. Therefore, the BSA-WS_2 is promising to be employed as contrast agents for CT imaging.

Conclusions

In summary, we develop a facial and eco-friendly method to synthesize WS_2 nanosheet as PTT agents. We also firstly employed these WS_2 nanosheets as the drug carrier to load photosensitizer MB for combined PTT and PDT treatment of cancer cells. The as-prepared WS_2 nanosheets could not only efficiently load photosensitizers but also regulate their singlet-oxygen generation by NIR irradiation, making them become a smart platform for the controllable regulation of photoactivity of PSs. The PDT, PTT and combined PTT-PDT effects of the WS_2 and BSA-WS_2@MB complex were evaluated and the efficacy of combined PDT-PTT treatment of cancer cells is significantly higher than PDT only and PTT only treatment. This clearly shows that the WS_2 nanosheets could be a multi-therapeutic platform that combines different therapeutic modalities to realize the synergistic effect for cancer therapy. Moreover, the WS_2 nanosheets featuring strong X-ray attenuation, also hold promise for CT imaging and thus may be approved as a multifunctional nanoplatform for simultaneous imaging-guided diagnosis and therapy.

Acknowledgements

This work was supported by National Basic Research Programs of China (973 program, No. 2012CB932504, 2011CB933403 and 2013CB933704), and National Natural Science Foundation of China (No. 21177128, 21277037 and 21101158).

References

1. Z. G. Zhou, B. Kong, C. Yu, X. Y. Shi, M. W. Wang, W. Liu, Y. N. Sun, Y. J. Zhang, H. Yang and S. P. Yang, *Sci. Reports*, 2014, **4**, 3653.
2. L. Cheng, K. Yang, Y. Li, J. Chen, C. Wang, M. Shao, S. T. Lee and Z. Liu, *Angew. Chem. Int. Ed. Engl.*, 2011, **50**, 7385-7390.
3. Z. M. Li, P. Huang, X. J. Zhang, J. Lin, S. Yang, B. Liu, F. Gao, P. Xi, Q. S. Ren and D. X. Cui, *Mol. pharmaceutics*, 2009, **7**, 94-104.
4. W. Tang, H. Xu, R. Kopelman and M. A. Philbert, *Photochem. Photobiol.*,

2005, **81**, 242-249.
5. G. Tian, W. L. Ren, L. Yan, S. Jian, Z. J. Gu, L. J. Zhou, S. Jin, W. Y. Yin, S. Li and Y. L.Zhao, *Small*, 2013, **9**, 1929-1938.
6. K. H. Bae, M. Park, M. J. Do, N. Lee, J. H. Ryu, G. W. Kim, C. Kim, T. G. Park and T. Hyeon, *ACS Nano*, 2012, **6**, 5266-5273.
7. P. Huang, Y. Kong, Z. Li, F. Gao and D. Cui, *Nanoscale Res. Lett.*, 2010, **5**, 949-956.
8. D. Wen, *Heat Transfer Eng.*, 2013, **34**, 1171-1179.
9. K. Pu, A. J. Shuhendler, J. V. Jokerst, J. G. Mei, S. S. Gambhir, Z. N. Bao and J. H. Rao, *Nat. Nanotechnology.*, 2014, **9**, 233-239.
10. D. K. Kirui, I. Khalidov, Y. Wang and C. A. Batt, *Nanomedicine*, 2013, **9**, 702-711.
11. A. Topete, M. Alatorre-Meda, P. Iglesias, E. M. Villar-Alvarez, S. Barbosa, J. A. Costoya, P. Taboada and V. Mosquera, *ACS Nano*, 2014, **8**, 2725-2738.
12. I. Roy, T. Y. Ohulchanskyy, H. E. Pudavar, E. J. Bergey, A. R. Oseroff, J. Morgan, T. J. Dougherty and P. N. Prasad, *J. Am. Chem. Soc.*, 2003, **125**, 7860-7865.
13. S. Kim, T. Y. Ohulchanskyy. H. E. Pudavar, R. K. Pandey and P. N. Prasad, *J. Am. Chem. Soc.*, 2007, **129**, 2669-2675.
14. S. Wang, R. Gao, F. Zhou and M. Selke, *J. Mater. Chem.*, 2004, **14**, 487-493.
15. D. Bechet, P. Couleaud, C. Frochot, M. L. Viriot, F. Guillemin and M. Barberi-Heyob, *Trends Biotechnol.*, 2008, **26**, 612-621.
16. E. S. Nyman and P. H. Hynninen, *J. Photoch. Photobio. B.*, 2004, **73**, 1-28.
17. P. Guardia, R. D. Corato, L. Lartigue, C. Wilhelm, A. Espinosa, M. Garcia-Hernandez, F. Gazeau, L. Manna and T. Pellegrino, *ACS Nano*, 2012, **6**, 3080-3091.
18. H. J. Jang, Y. K. Kim, H. Huh and D. H. Min, *ACS Nano*, 2014, **8**, 467-475.
19. J. Lin, S. J. Wang, P. Huang, Z. Wang, S. H. Chen, G. Niu, W. W. Li, J. He, D. X. Cui, G. M. Lu, X. Y. Chen and Z. H. Nie, *ACS Nano*, 2013, **7**, 5320-5329.
20. Z. Fan, X. Dai, Y. Lu, E. Yu, N. Brahmbatt, N. Carter, C. Tchouwou, A. K. Singh, Y. Jones, H. Yu and P. C. Ray, *Mol. Pharm.*, 2014, **11**, 1109-1116.
21. S. Khan, F. Alam, A. Azam and A. U. Khan, *Int. J. Nanomed.*, 2012, **7**, 3245-3257.
22. Y. Su, X. Wei, F. Peng, Y. Zhong, Y. Lu, S. Su, T. Xu, S. T. Lee and Y. He, *Nano. Letter.*, 2012, **12**, 1845-1850.
23. B. Jang, J. Y. Park, C. H. Tung, I. H. Kim and Y. Choi, *ACS Nano*, 2011, **5**, 1086-1094.
24. Z. Zhang, J. Wang and C. Chen, *Adv. Mater.*, 2013, **25**, 3869-3880.
25. L. Gao, J. B. Fei, J. Zhao, H. Li, Y. Cui and J. B. Li, *ACS Nano*, 2012, **6**, 8030-8040.
26. J. Gautier, E. Allard-Vannier, E. Munnier, M. Souce and I. Chourpa, *J. Controlled Release*, 2013, **169**, 48-61.
27. P. Huang, J. Lin, X. Wang, Z. Wang, C. Zhang, M. He, K. Wang, F. Chen, Z. Li, G. Shen, D. Cui and X. Chen, *Adv. Mater.*, 2012, **24**, 5104-5110.

28. X. Wang, C. Wang, L. Cheng, S. T. Lee and Z. Liu, *J. Am. Chem. Soc.*, 2012, **134**, 7414-7422.
29. X. Liu, H. Tao, K. Yang, S. Zhang, S. T. Lee and Z. Liu, *Biomaterials*, 2011, **32**, 144-151.
30. Z. Zhu, Z. W. Tang, J. A. Phillips, R. H. Yang, H. Wang and W. H. Tan, *J. Am. Chem. Soc.*, 2008, **130**, 10856-10857.
31. M. Zhou, R. Zhang, M. Huang, W. Lu, S. Song, M. P. Melancon, M. Tian, D. Liang and C. Li, *J. Am. Chem. Soc.*, 2010, **132**, 15351-15358.
32. Q. W. Tian, F. Jiang, R. J. Zou, Q. Liu, Z. G. Chen, M. F. Zhu, S. P. Yang, J. L. Wang, J. H. Wang, and J. Q. Hu, *ACS Nano*, 2011, **5**, 9761-9771.
33. S. Ramadan, L. Guo, Y. Li, B. Yan and W. Lu, *Small*, 2012, **8**, 3143-3150.
34. Q. Tian, M. Tang, Y. Sun, R. Zou, Z. Chen, M. Zhu, S. Yang, J. Wang, J. Wang and J. Hu, *Adv. Mater.*, 2011, **23**, 3542-3547.
35. J. Hu, G. Song, L. Han, W. Zou, Z. Xiao, X. Huang, Z. Qin and R. Zou, *Nano-Micro Lett.*, 2014, **6**.169-177.
36. Z. Zha, S. Wang, S. Zhang, E. Qu, H. Ke, J. Wang and Z. Dai, *Nanoscale*, 2013, **5**, 3216-3219.
37. Q. Xiao, X. Zheng, W. Bu, W. Ge, S. Zhang, F. Chen, H. Xing, Q. Ren, W. Fan, K. Zhao, Y. Hua and J. Shi, *J. Am. Chem. Soc.*, 2013, **135**, 13041-13048.
38. Y. Wang, H. Wang, D. Liu, S. Song, X. Wang and H. Zhang, *Biomaterials*, 2013, **34**, 7715-7724.
39. A. Sahu, W. I. Choi, J. H. Lee and G. Tae, *Biomaterials*, 2013, **34**, 6239-6248.
40. Y. Wang, K. Wang, J. Zhao, X. Liu, J. Bu, X. Yan and R. Huang, *J. Am. Chem. Soc.* 2013, **135**, 4799-4804.
41. J. Oh, H. Yoon and J. H. Park, *Biomedic. Eng. Lett.*, 2013, **3**, 67-73.
42. S. Wang, P. Huang, L. Nie, R. Xing, D. Liu, Z. Wang, J. Lin, S. Chen, G. Niu, G. Lu and X. Chen, *Adv. Mater.*, 2013, **25**, 3055-3061.
43. L. Cheng, J. Liu, X. Gu, H. Gong, X. Shi, T. Liu, C. Wang, X. Wang, G. Liu, H. Xing, W. Bu, B. Sun and Z. Liu, *Adv. Mater.*, 2014, **26**, 1886-1893.
44. T. Liu, C. Wang, X. Gu, H. Gong, L. Cheng, X. Shi, L. Feng, B. Sun and Z. Liu, *Adv. Mater.*, 2014, DOI: 10.1002/adma.201305256.
45. C. F. Zhu, Z. Y. Zeng, H. Li, F. Li, C. H. Fan and H. Zhang, *J. Am. Chem. Soc.* 2013, **135**, 5998-6001.
46. J. Lin, S. J. Wang, P. Huang, Z. Wang, S. H. Chen, G. Niu, W. W. Li, J. He, D. X. Cui, G. M. Lu, X. Y. Chen and Z. H. Nie, *ACS Nano*, 2013, **7**, 5320-5329.
47. Q. W. Tian, F. R. Jiang, R. J. Zou, Q. Liu, Z. G. Chen, M. F. Zhu, S. P. Yang, J. L. Wang, J. H. Wang and J. Q. Hu., *ACS Nano*, 2011, **5**, 9761-9771.
48. J. P. Tardivo, A. D. Giglio, C. S. Oliveira, D. S. Gabrielli, H. C. Junqueira, D. B. Tada, D. Severino, R. F. Turchiello and M. S. Baptista, *Photodiagn. Photodyn.*, 2005, **2**, 175-191.
49. Q. Chen, C. Wang, L. Cheng, W. W. He, Z. P. Cheng, Z. Liu, *Biomaterials,* 2014, **35**, 2915-2923.

Figure

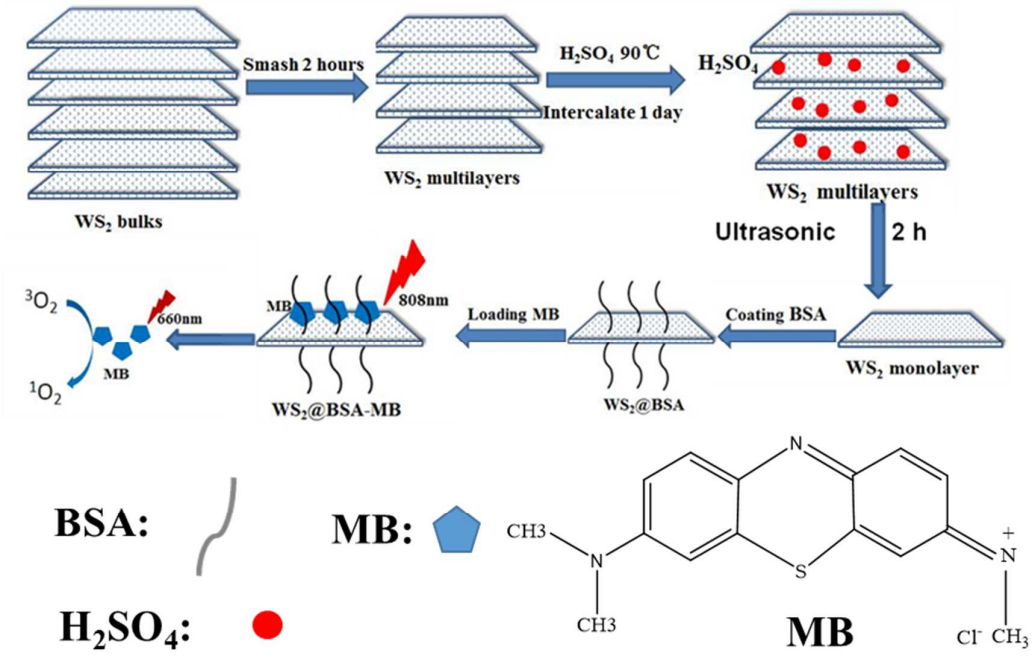

Scheme 1. Schematic illustration of the synthetic procedure of WS_2 nanosheets and their applications as a multifunctional photosensitizer delivery system for combining photothermal and photodynamic therapy of cancer.

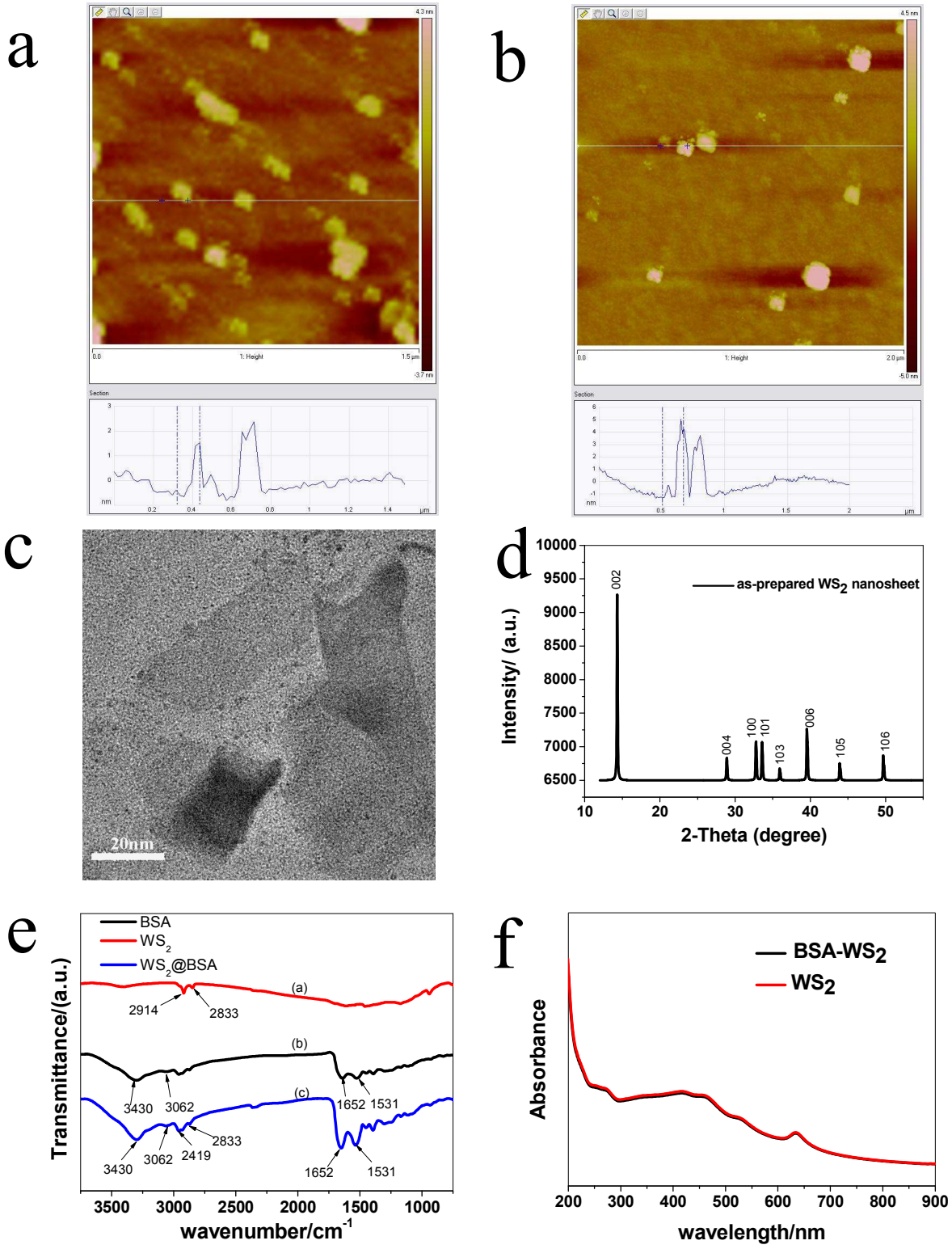

Figure 1. AFM topography images of the as-made WS_2 nanosheets (a) and BSA coated WS_2 (b). (c) TEM image of the synthesized WS_2 nanosheets. (d) XRD pattern of the as-obtained WS_2 nanosheets. (e) The FT-IR spectra of WS_2 nanosheets (WS_2), bovine serum albumin (BSA), and the BSA functionalized WS_2 nanosheets (BSA-WS_2). (f) The UV-VIS spectra of the WS_2 nanosheets before and after BSA coating.

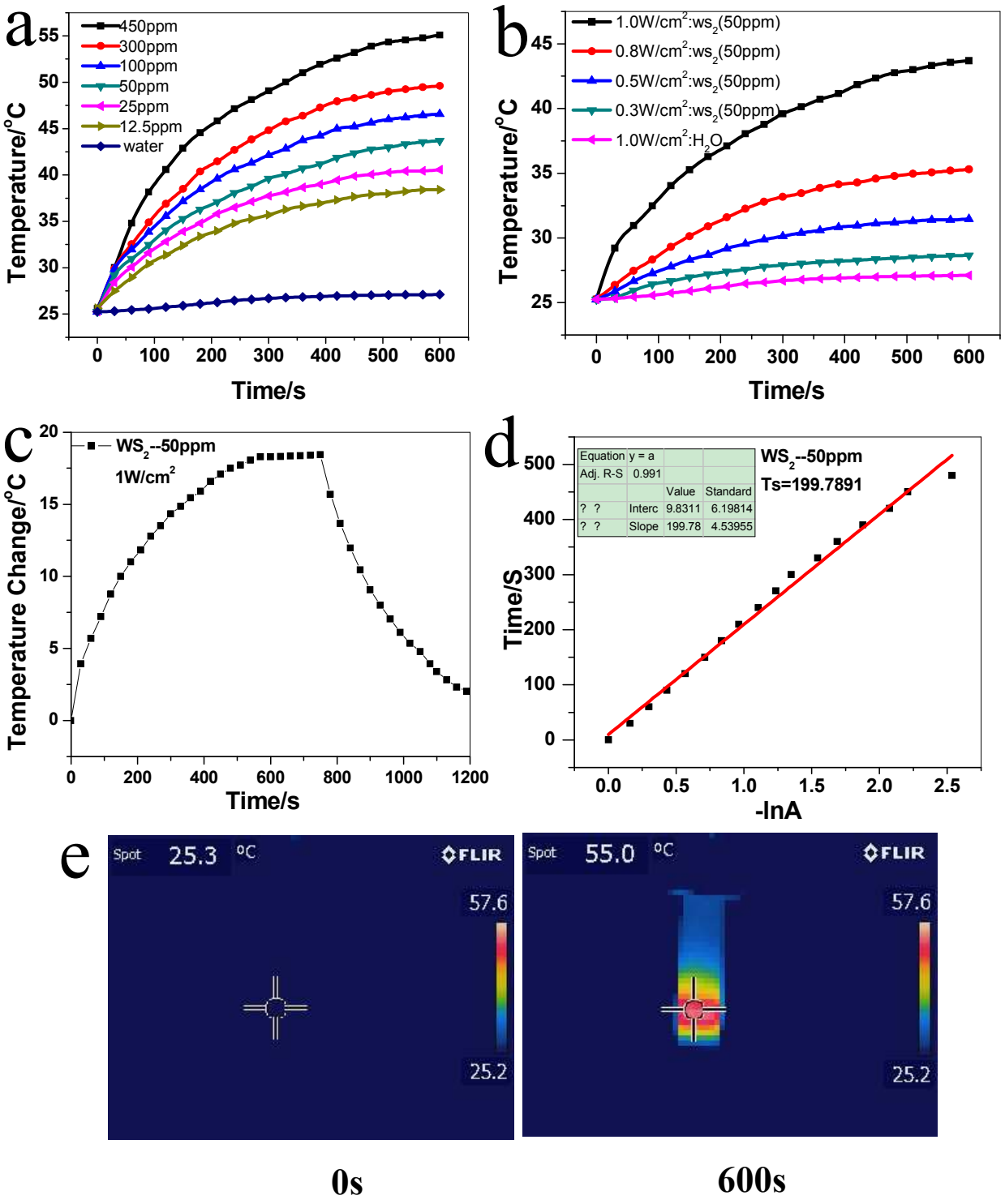

Figure 2. (a) The temperature evaluation of pure water and the aqueous dispersion of WS_2 nanosheets with different concentration (12.5, 25, 50, 100, 300, 450 ppm) as a functional of irradiation time (0-10min) of 808nm laser with power density of 1.0 W/cm^2 under room temperature. (b) The temperature evaluation of the aqueous dispersion of WS_2 nanosheets (50 ppm) as a functional of irradiation time (0-10 min)

of 808nm laser with different power density (0.3, 0.5, 0.8, 1.0 W/cm^2), and the pure water was used as a negative control. (c) Photothermal response of the aqueous dispersion of WS_2 nanosheets (50 ppm) with the NIR laser (808 nm, 1.0 W/cm^2) irradiation for 13 min, and then shut off the laser. (d) Linear time data versus–lnθ obtained from the cooling period of figure 2d. (e) IR images of the WS_2 nanosheets solution before and after 808 nm laser irradiation at a power density of 1 W/cm^2 for 10 min.

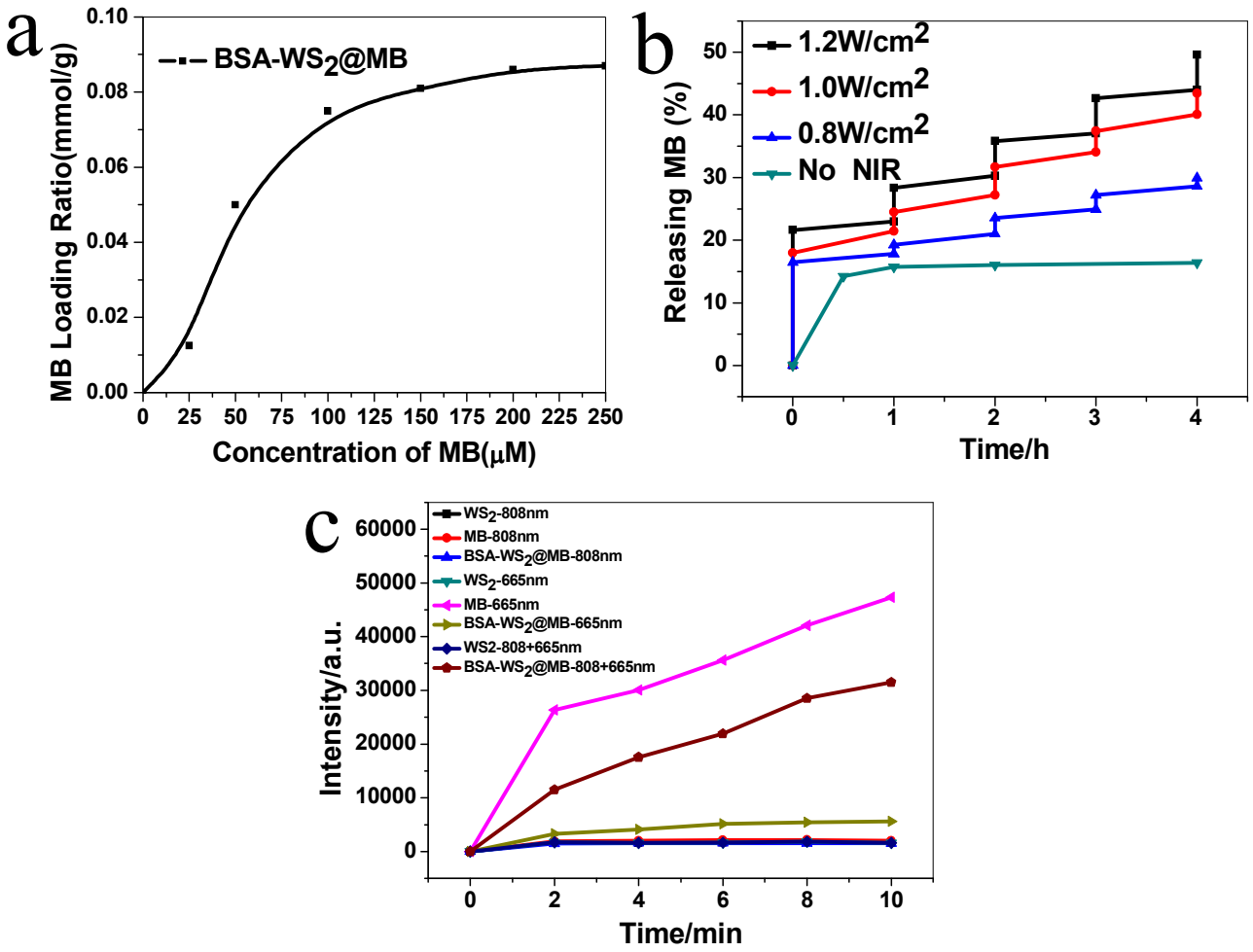

Figure 3. Photosensitizer loading and releasing behaviors (a) plots of loading amount of the photosensitizer methylene blue (MB) to WS_2 nanosheets at different concentrations. (b) MB releasing from MB-loaded WS_2 complex at an 808 nm laser irradiation with different output power density (1.2, 1.0, 0.8 W/cm^2, respectively). (c) The time-course generation of singlet oxygen by measuring the increase fluorescence intensity of SOSG at the characteristic peak of 530nm as a functional of 665 nm LED lamp irradiation time. The output power density and irritation time of 808 nm laser for all samples were fixed at 1W/cm^2 and 15 min, respectively. The irradiation of 665 nm LED lamp was carried out after the 808 nm irradiation treatments and the power output of 665 nm LED lamp for all samples were fixed at 50 mW/cm^2.

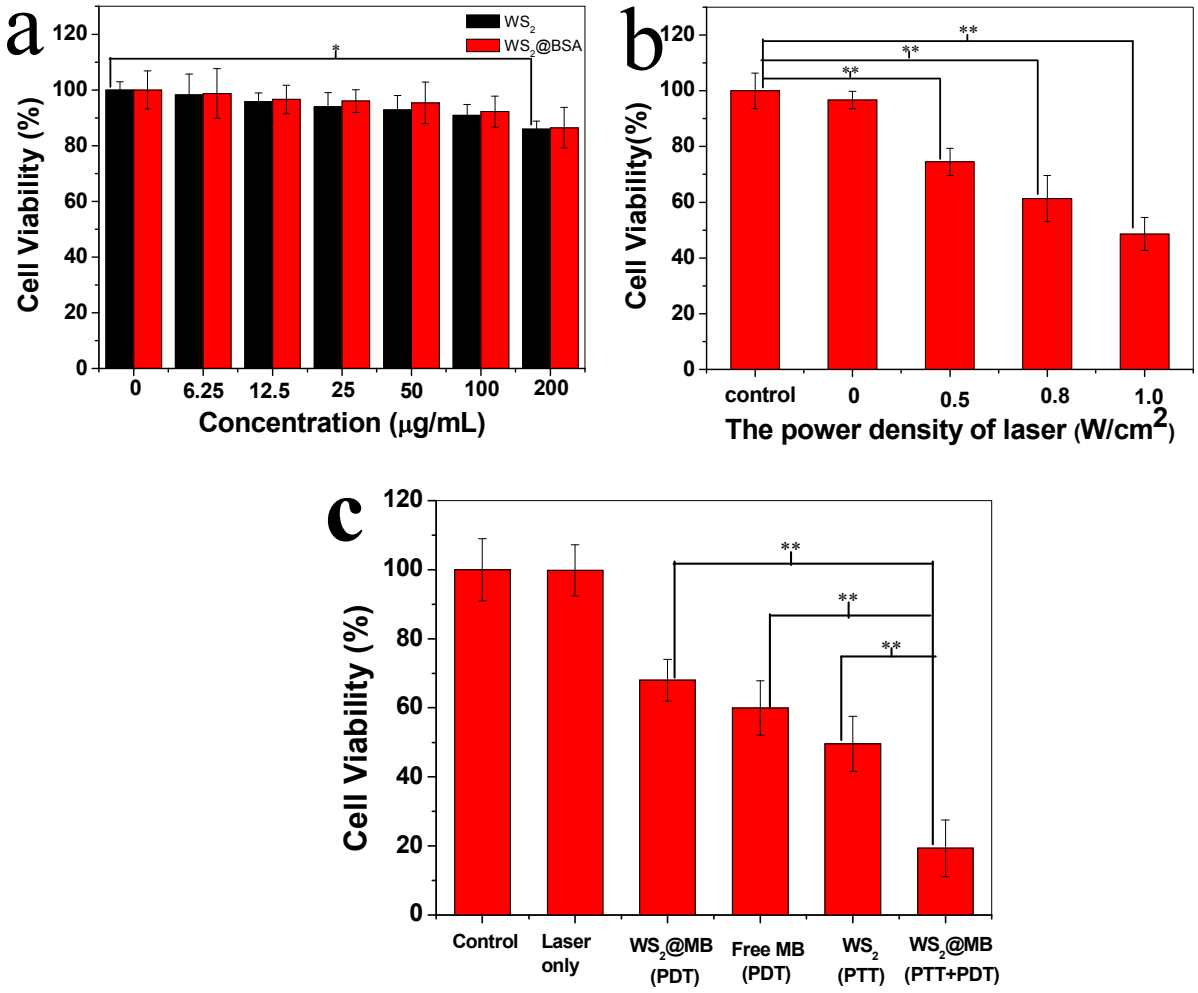

Figure 4. (a)Cell viability of HeLa incubated with WS_2 and BSA-WS_2 at various concentrations for 24 h without light interference, respectively. (b) In vitro cytotoxicity effect of WS_2 induced by PTT, showing the higher laser power density induce the higher cytotoxicity. (c) *In vitro* cytotoxicity effect of PDT, PTT, and PTT+PDT. The output power of 808 nm laser and 665 nm LED lamp for all tests are fixed at 1W/cm^2 for 15 min and 50mW/cm^2 for 5 min, respectively. Error bars were based on SD of six parallel samples. *P* values were carried out by the student's test: * $P < 0.05$, * * $P < 0.001$.

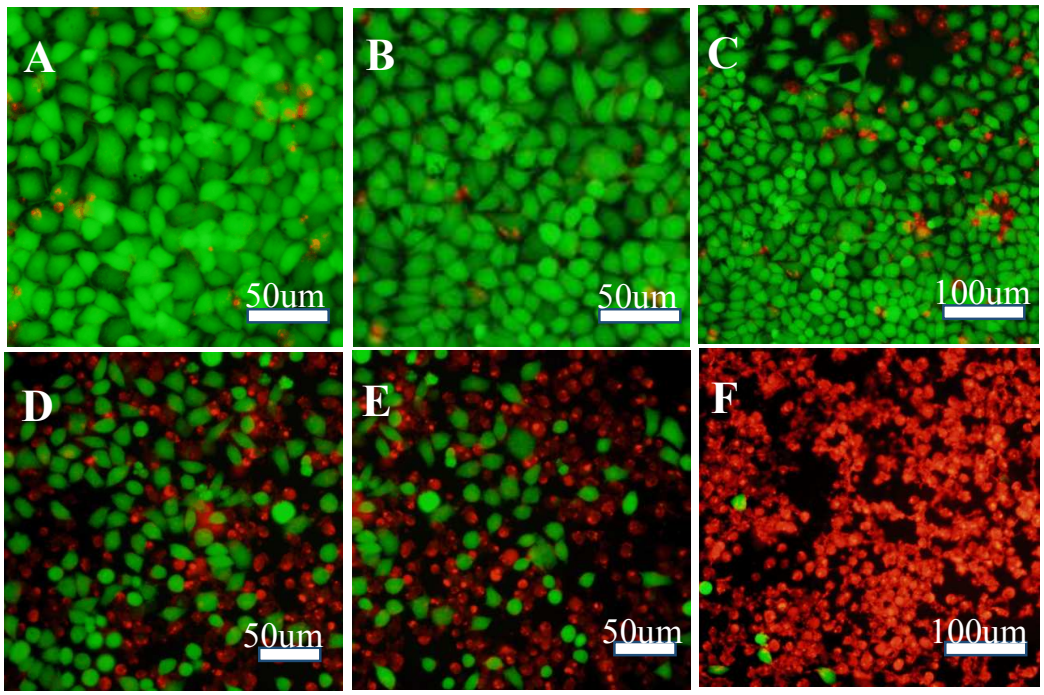

Figure 5. Fluorescent images of HeLa cells incubated with (A) WS_2, (B)BSA-WS_2, (C)Laser only (808-nm LED+665-nm LED), (D)WS_2@MB+665-nm LED, (E)WS_2+808-nm laser, (F)WS_2@MB+808-nm laser+665-nm LED for 2 h after live-dead cells staining. Green indicates live cells and red represents the dead ones. The concentration of WS_2@MB was fixed at 100 μg/ mL. And the 808-nm laser (1W/cm^2) and 665-nm LED (50 mW/cm^2) irradiation was kept for 15 min and 5 min, respectively.

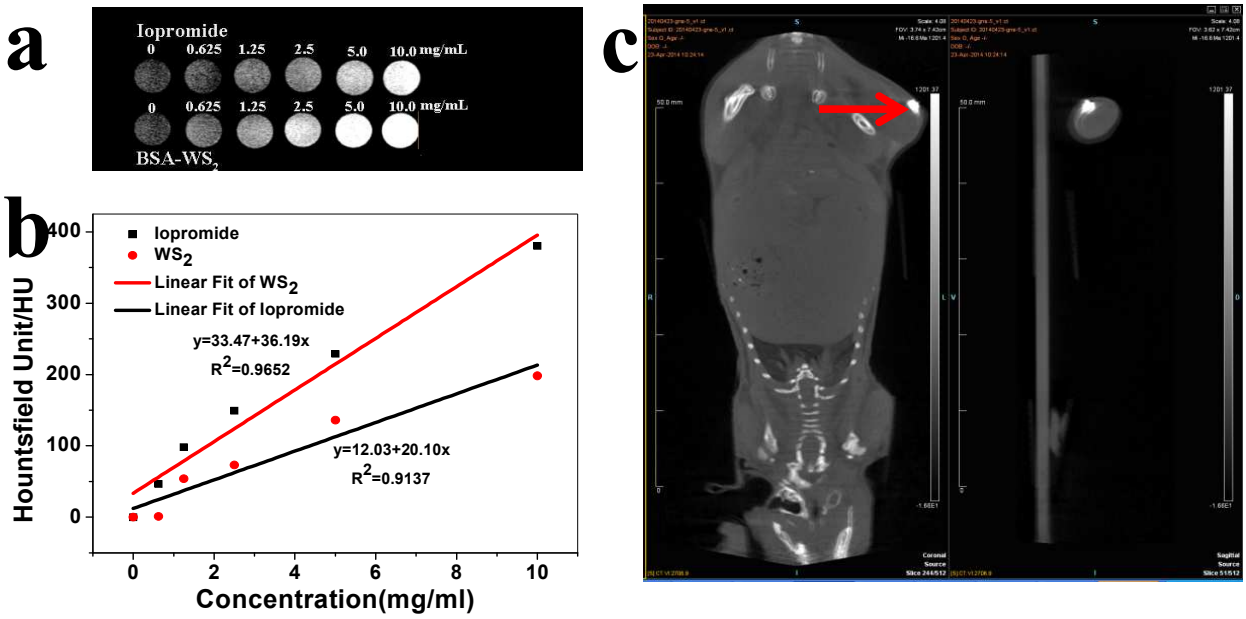

Figure 6. (a) *in vitro* CT images of Iopromide and BSA-WS_2 aqueous solutions with different concentrations. (b) Hountsfied Unit values of BSA-WS_2 and Iopromide as the function of their concentrations. (c) *In vivo* CT image of a Balb/c nude mice after intratumor injection with 3 mg/ mL BSA-WS_2 nanosheets.